

# A nanoparticle stored with an atomic ion in a linear Paul trap

Dmitry S. Bykov,<sup>1\*</sup> Lorenzo Dania,<sup>1†</sup> Florian Goschin,<sup>1</sup> Tracy E. Northup<sup>1</sup>

<sup>1</sup>Institut für Experimentalphysik, Universität Innsbruck  
Technikerstraße 25, 6020 Innsbruck, Austria

\*To whom correspondence should be addressed; E-mail: dmitry.bykov@uibk.ac.at

†Present address: Photonics Laboratory, ETH Zürich, CH-8093 Zürich, Switzerland

**Radiofrequency traps are used to confine charged particles but are only stable for a narrow range of charge-to-mass ratios. Here, we confine two particles—a nanoparticle and an atomic ion—in the same radiofrequency trap although their charge-to-mass ratios differ by six orders of magnitude. The confinement is enabled by a dual-frequency voltage applied to the trap electrodes. We introduce a robust loading procedure under ultra-high vacuum and characterize the stability of both particles. It is observed that slow-field micromotion, an effect specific to the dual-field setting, plays a crucial role for ion localization and will be important to account for when engineering controlled interactions between the particles.**

## Introduction

The confinement of charged particles in radiofrequency (RF) traps is a fundamental technique for mass spectrometry (1), cold molecular chemistry (2), and quantum information processing (3–5) and has wide-ranging applications from the study of condensed-matter material prop-

erties (6) to the detection of millicharged dark matter (7). Typically, a trap is configured to levitate a specific object with a predefined charge-to-mass ( $Q/m$ ) ratio. However, certain applications require interactions between different objects in the same trap. Examples include highly controlled reactions between cold molecular ions (8), sympathetic cooling of one ion species with another (9, 10), and quantum logic spectroscopy (11–14).

While the  $Q/m$  selectivity of RF traps is advantageous for certain applications, such as mass spectrometry, it limits the range of objects that can be confined simultaneously in the same trap. To overcome this limitation and trap two species with very different  $Q/m$  ratios, a Paul trap driven by two voltage sources has been proposed (15–17), targeting antihydrogen synthesis (15, 17) and sympathetic cooling of megadalton particles, including nanoparticles or viruses (16). In this scenario, the frequency and amplitude of each voltage source are tuned to provide confinement for a particle with a specific  $Q/m$  ratio without compromising the stability of the second species.

Here, we experimentally demonstrate a dual-frequency linear Paul trap driven by 17.5 MHz and 7 kHz voltage sources. This approach allows us to confine a silica nanoparticle and atomic calcium ions in the same RF trap, thus creating a hybrid system consisting of an ultra-high-quality-factor mechanical oscillator (18) and an atomic qubit. The trapped objects differ by six orders of magnitude in their  $Q/m$  ratio and by eight orders of magnitude in mass.

## Theoretical background

Let us examine the conditions for stable trapping of a particle—either a nanoparticle or an atomic ion—in the quadrupole electric potential  $\Phi$  of a linear Paul trap driven by two voltage sources. In a coordinate system with the origin at the trap’s geometric center, the potential in

the  $xy$  plane orthogonal to the trap axis can be written as

$$\Phi(x, y) = (V_{\text{slow}} \cos \Omega_{\text{slow}} t + V_{\text{fast}} \cos \Omega_{\text{fast}} t) \frac{x^2 - y^2}{2r_0^2}, \quad (1)$$

where  $r_0 = 0.9$  mm is the characteristic distance from the electrodes to the trap axis,  $\Omega_{\text{slow}}$  and  $\Omega_{\text{fast}}$  are the two frequencies of the drive voltages, and  $V_{\text{slow}}$  and  $V_{\text{fast}}$  are their amplitudes. First, we focus on the motion of a nanoparticle along one axis; our goal is to compare the influence of the slow and fast components. The equation of motion along  $x$  is

$$m_{(n)} \ddot{x} = -Q_{(n)} (V_{\text{slow}} \cos \Omega_{\text{slow}} t + V_{\text{fast}} \cos \Omega_{\text{fast}} t) \frac{x}{r_0^2}, \quad (2)$$

where  $m_{(n)}$  and  $Q_{(n)}$  are the mass and charge of the nanoparticle. If we neglect the fast field and work in the pseudopotential approximation, the oscillation frequency in the effective trap potential can be written as (19)

$$\omega_{(n)}|_{\Omega_{\text{slow}}} = \frac{\Omega_{\text{slow}} q_{(n)}}{2\sqrt{2}}, \quad (3)$$

where we have introduced the stability parameter

$$q_{(n)} = \frac{2Q_{(n)} V_{\text{slow}}}{m_{(n)} r_0^2 \Omega_{\text{slow}}^2}. \quad (4)$$

If, on the other hand, we neglect the slow field, the resonance frequency can be expressed as a fraction of the frequency calculated in Eq. 3:

$$\omega_{(n)}|_{\Omega_{\text{fast}}} = \frac{\Omega_{\text{slow}}}{\Omega_{\text{fast}}} \frac{V_{\text{fast}}}{V_{\text{slow}}} \omega_{(n)}|_{\Omega_{\text{slow}}} \approx 10^{-2} \omega_{(n)}|_{\Omega_{\text{slow}}}, \quad (5)$$

where the approximation in the final step is based on typical voltages used in the experiment. From Eq. 5, we conclude that the fast field acts only as a perturbation to the motion of the nanoparticle, which is confined by the slow field, and that no special conditions are imposed on the field parameters.

Next, we turn to the equation of motion of an ion in the dual-frequency field:

$$m_{(i)} \ddot{x} = -e(V_{\text{slow}} \cos \Omega_{\text{slow}} t + V_{\text{fast}} \cos \Omega_{\text{fast}} t) \frac{x}{r_0^2}, \quad (6)$$

where  $m_{(i)}$  is the mass and  $e$  the elementary charge. Under the condition  $\Omega_{\text{slow}} \ll \Omega_{\text{fast}}$ , the slow field acts as a slowly varying DC force, and it is possible to map the ion's equation of motion to the Mathieu equation

$$\ddot{x} + (a_{\text{eff}} + 2q_{(i)} \cos 2t)x = 0 \quad (7)$$

for the stability parameters

$$a_{\text{eff}} = \frac{4eV_{\text{slow}}}{m_{(i)}r_0^2\Omega_{\text{fast}}^2}, \quad (8)$$

$$q_{(i)} = \frac{2eV_{\text{fast}}}{m_{(i)}r_0^2\Omega_{\text{fast}}^2}. \quad (9)$$

For  $q_{(i)} \ll 1$ , the stability condition for solutions of the Mathieu equation is approximately (4)

$$|a_{\text{eff}}| < q_{(i)}^2/2. \quad (10)$$

Thus, Eq. 10 imposes conditions on the fast and slow fields with which co-trapping of a nanoparticle and an ion is possible.

## Experimental approach

We implement the dual-frequency trap by applying a voltage oscillating at  $\Omega_{\text{fast}} = 17.5$  MHz to one pair of RF electrodes and a second voltage at  $\Omega_{\text{slow}} = 7$  kHz to a second pair. (A similar configuration is described in Ref. (20) for an experiment with  $^{40}\text{Ca}^+$  ions.) The trap schematic is shown in Fig. 1a. The fast voltage signal at  $\Omega_{\text{fast}}$  is provided by a low-noise function generator (Rohde&Schwarz SMB100B) and preamplified by a high-power amplifier (Mini-Circuits LZY-22+). We supply the pre-amplified signal to a tap of the inductive coil of a resonant LC circuit in which the trap electrodes act as a capacitance. In the case of the slow voltage at  $\Omega_{\text{slow}}$ , a different function generator drives a low-noise, high-voltage amplifier (Trek PZD700A). The internal resistance of the slow voltage source and a 4.7 nF capacitor act as a low-pass filter, effectively grounding the fast signal. The slow field sees this capacitor as an open circuit.

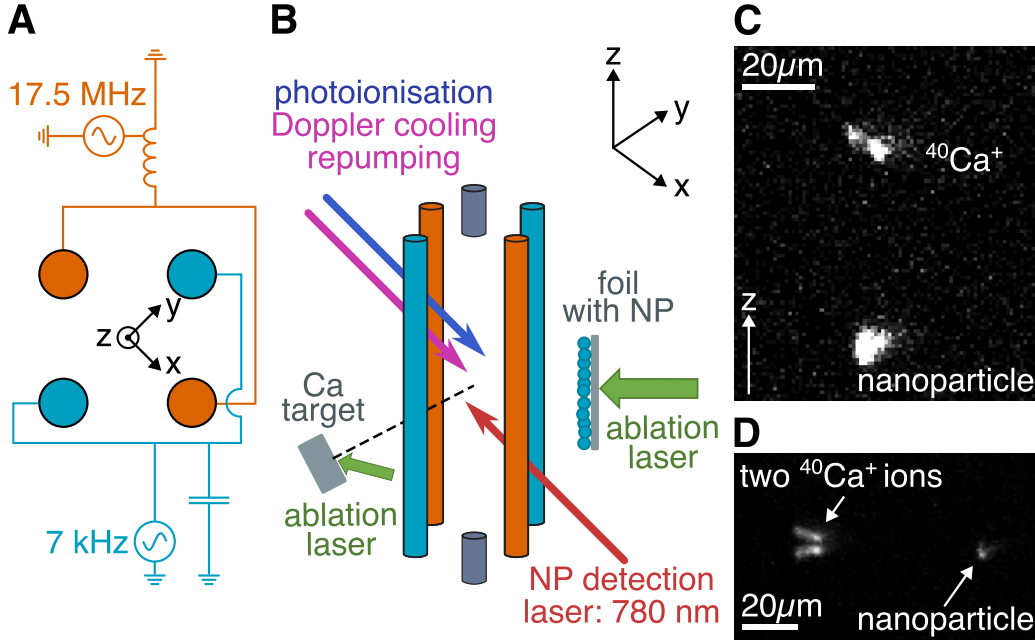


Figure 1: Experimental setup. (a) Dual-frequency drive of the linear Paul trap. (b) Schematic of the procedure for trapping a nanoparticle (NP) and an ion. Along the  $z$  axis, DC endcap electrodes are indicated in gray. Not shown: two pairs of compensation electrodes for displacement in the  $xy$  plane. (c) Camera image of a  $^{40}\text{Ca}^+$  ion and a nanoparticle confined in the same Paul trap. (d) A second image in which two ions are confined with a nanoparticle.

Similarly, the inductor of the resonant circuit acts as a high-pass filter, effectively grounding the slow signal.

As a first step, a nanoparticle is loaded into the trap under ultra-high vacuum via laser-induced acoustic desorption (LIAD) (21, 22) combined with temporal control of the Paul-trap potential (23). The nanoparticle source is a 300  $\mu\text{m}$  thick aluminum foil with silica nanospheres deposited on the front side; the spheres have a nominal diameter of 300 nm. A pulsed ablation laser (4 mJ, 5 ns) is focused on the back side of the foil (Fig. 1b). The geometry of the trap and the source are as described in Ref. (23), with the exception that here, the distance between DC endcap electrodes is 3.4 mm. At this stage, only the slow voltage at  $\Omega_{\text{slow}}$  is applied to the trap electrodes, with amplitude  $V_{\text{slow}} = 1.4 \text{ kV}_{\text{pp}}$ . The endcap voltage is 400 V.

After loading, we cool the nanoparticle's motion using electrical feedback based on opti-

cal detection at 780 nm. There are two differences with respect to the protocol of Ref. (24): First, the nanoparticle’s position along the  $x$ ,  $y$ , and  $z$  axes is detected with a confocal setup implemented with fiber-coupled avalanche photodiodes (APDs) (22, 25–27). Second, the  $x$ - and  $y$ -axis feedback signals are combined and sent to a feedback electrode mounted next to the trap, but the  $z$ -feedback signal is sent to the lower endcap electrode through a high-pass filter. Feedback cooling operates continuously during the subsequent steps.

Next, we increase the nanoparticle charge  $Q_{(n)}$ . Recall from Eq. 10 that the values of  $V_{\text{slow}}$  compatible with co-trapping an ion are bounded from above; a higher value of  $Q_{(n)}$  allows the stiffness of the nanoparticle’s trap to be maintained while  $V_{\text{slow}}$  is reduced (see Eqs. 3 and 4). When the ablation laser is directed with a pulse energy of 1 mJ to a pure calcium target near the trap (Fig. 1b), it is observed that  $Q_{(n)}$  increases and saturates at around 300  $e$  in the absence of a fast field. The presence of a fast field allows even higher values of  $Q_{(n)}$  to be obtained during this process. Thus, at this point we introduce the fast field with  $V_{\text{fast}} \approx 1.5 \text{ kV}_{\text{pp}}$ . One to three pulses of the ablation laser corresponds to an increase of a few elementary charges; we periodically interrupt this stepwise process to reduce  $V_{\text{slow}}$  such that the  $q_{(n)}$  parameter remains below 0.9. We stop the charging process at an amplitude  $V_{\text{slow}} = 160 \text{ V}_{\text{pp}}$ , for which  $Q_{(n)} \approx 800 \text{ e}$  is reached.

Once the nanoparticle has been localized and its charge increased, we load a  $^{40}\text{Ca}^+$  ion into the dual-frequency trap. First, all laser beams required for ion loading, cooling, and detection are aligned to the geometric center of the trap. Here, the trapped nanoparticle serves as a scattering target onto which the attenuated beams are focused. Next, the amplitude of the fast voltage is set to  $2.5 \text{ kV}_{\text{pp}}$ . The voltage on one of the trap’s two pairs of compensation electrodes is then increased such that the nanoparticle is displaced in the  $xy$  plane, making room for the ion at the trap center. (As the ion’s charge is three orders of magnitude smaller than the nanoparticles’s charge, its equilibrium position is less affected by the compensation field.) The nanoparticle-detection optics and the feedback-cooling parameters are adjusted to account

for this new position. Finally, we operate the ablation laser, still focused on the calcium target, at a pulse energy of 0.5 mJ in conjunction with diode lasers at 375 nm and 423 nm for two-step isotope-selective photoionization (28, 29). Once an ion is loaded, it is detected and Doppler-cooled via fluorescence on the 397 nm  $4^2S_{1/2} \leftrightarrow 4^2P_{1/2}$  transition, with repumping on the 866 nm  $4^2P_{1/2} \leftrightarrow 3^2D_{3/2}$  and 854 nm  $4^2P_{3/2} \leftrightarrow 3^2D_{5/2}$  transitions. All three diode-laser frequencies are locked to a wavemeter.

To verify that a nanoparticle and an atomic ion are co-trapped, we illuminate them with the 397 nm, 866 nm, and 854 nm laser fields and capture their image using an electron multiplying charge-coupled device (EM-CCD) camera. An example image is shown in Fig. 1c: nanoparticle and ion are separated by  $55(10) \mu\text{m}$ . The laser beams are focused on the ion, and the nanoparticle is in the tail of the Gaussian intensity profile; the camera detects elastically scattered light from the nanoparticle. Only 397 nm light is used for imaging, and an optical bandpass filter (Thorlabs FBH400-40) in front of the camera removes other wavelengths.

## Experimental results

### Co-trapping conditions

To determine whether the theoretical description above is consistent with our demonstration of co-trapping, we characterize the stability of nanoparticle and ion separately in the dual-frequency Paul trap. First, a nanoparticle is confined solely with the slow voltage. The fast voltage is then added with increasing amplitude up to  $2.5 \text{ kV}_{\text{pp}}$  while the position and oscillation frequency of the nanoparticle are monitored with a camera and the confocal detection setup, respectively. We find that the nanoparticle remains trapped for all amplitudes and that the presence of the fast voltage increases the nanoparticle's 1 kHz frequency in the  $xy$  plane by 10 Hz for  $V_{\text{slow}} = 2.5 \text{ kV}_{\text{pp}}$ . These observations are in agreement with Eq. 5.

Next, the ion is confined for several values of  $V_{\text{fast}}$ . At each setting,  $V_{\text{slow}}$  is increased until the

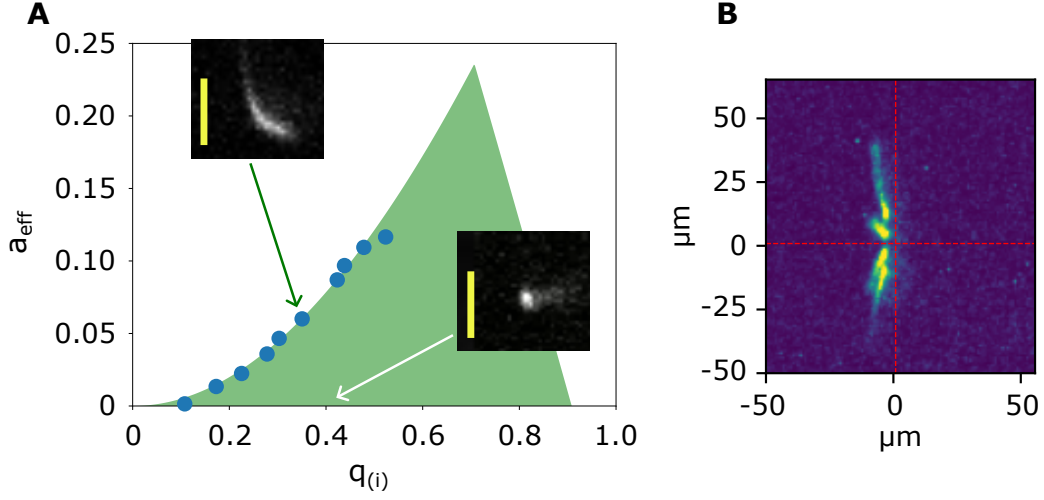


Figure 2: Influence of the slow field on the ion. (a) Blue dots: instability threshold measured with the ion, plotted in terms of the stability parameters  $q_{(i)}$  and  $a_{\text{eff}}$ . Green area: Strutt diagram, calculated from experimental parameters. Insets are camera images of the ion for different stability regimes; the scale bar is  $10 \mu\text{m}$ . (b) Composite image of the ion at four positions along the  $z$  axis for  $q_{(i)} = 0.4$ ,  $a_{\text{eff}} = 0.06$ .

ion is expelled from the trap; this threshold amplitude is identified as  $V_{\text{slow}}^{\text{max}}$ . In Fig. 2a, the pair of stability parameters  $(q_{(i)}, a_{\text{eff}})$  is plotted for each pair  $(V_{\text{fast}}, V_{\text{slow}}^{\text{max}})$ . Superimposed on these data points is a Strutt diagram (4) calculated from the solutions to the Mathieu equation, Eq. 7. We see that the experimentally determined thresholds lie at the edge of the Strutt diagram's stable region, consistent with our expectations. The rightmost data point, at  $q_{(i)} = 0.55$ , corresponds to  $(V_{\text{fast}} = 2.5 \text{ kV}_{\text{pp}}, V_{\text{slow}}^{\text{max}} = 260 \text{ V}_{\text{pp}})$ , providing an upper bound for the value of  $V_{\text{slow}}$  at which ions can be loaded.

Camera images provide further evidence of the slow field's influence on ion confinement: the two insets of Fig. 2a show that an ion is well localized when the trap is operated deep in the stable region of the Strutt diagram, but that its position extends over several tens of micrometers at the instability threshold. This elongation is due to micromotion—not the well-known micromotion at  $\Omega_{\text{fast}}$  in a single-frequency RF trap (19), but at the second frequency  $\Omega_{\text{slow}}$ . Figure 2b is a composite of four images of this slow-frequency micromotion in the



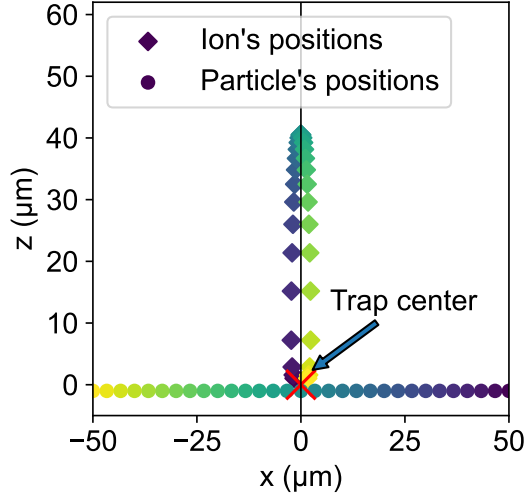


Figure 3: Ion-particle interaction. Circles: fixed nanoparticle positions in the dual-frequency trap. Diamonds: each ion position is calculated from the corresponding nanoparticle position. Ion-nanoparticle pairs are indicated with the same color. Calculation parameters: the nanoparticle's charge is  $800 e$ , and the ion's secular frequencies along the  $x$  and  $z$  axes are  $\omega_{(i),x} = 4 \text{ MHz}$ ,  $\omega_{(i),z} = 1 \text{ MHz}$ .

stable region, each obtained for a different position of the ion along the  $z$  axis, set by the endcap voltage. We see that the micromotion amplitude increases as the ion is displaced further from the origin. This image underscores the importance of positioning the ion at the slow-micromotion minimum. For future experiments based on the controlled interaction of two particles in a dual-frequency trap, it will be crucial to analyze the impact of slow micromotion.

Having examined the nanoparticle and ion separately, we turn to the question of where the two particles are located when they are trapped together. Recall, for example, that in the loading procedure, it was necessary to position the nanoparticle such that the ion would be loaded at the trap center, to which the lasers had been aligned. In Fig. 3, we calculate the equilibrium position of the ion for different positions of the nanoparticle, using typical experimental parameters. The ion position is determined by the trap potential, Coulomb repulsion from the charged nanoparticle, and the DC compensation-electrode voltages  $V_{c1}$  and  $V_{c2}$ . Here, fixing the nanoparticle

position as an input parameter in the calculation is equivalent to fixing  $V_{c1}$  and  $V_{c2}$ . The nanoparticle positions are chosen to lie on the line ( $-50 \mu\text{m} \leq x \leq 50 \mu\text{m}, y = 0 \mu\text{m}, z = -1 \mu\text{m}$ ), where the small displacement along  $z$  breaks the symmetry of the nanoparticle with respect to the endcaps, ensuring that the ion will be found in the half-space  $z \geq -1$ . In practice, this displacement is at the resolution limit of our imaging system. Consider the case of a nanoparticle at  $x = \pm 50 \mu\text{m}$ : the ion is found near the origin, and we infer that the interaction between nanoparticle and ion is negligible compared to the interaction with the trap. As the nanoparticle is brought closer to the origin, the ion is displaced along the  $z$  axis, indicating that the particles' interaction has become significant. Thus, this calculation provides intuition for how the competing forces are balanced. It also highlights that there are two ways to trap an ion at the origin, which, as we have just seen, minimizes its micromotion at  $\Omega_{\text{slow}}$ : the nanoparticle must be displaced either in the  $xy$  plane or along the  $z$  axis.

## Localization and manipulation of ions and nanoparticles

Let us refer to the case of nanoparticle displacement in the  $xy$  plane as an  $xy$  pair and to the case of displacement along the  $z$  axis as a  $z$  pair. Examples of the two configurations are shown in Figs. 4a and b. The nanoparticle in an  $xy$  pair experiences excess micromotion and is more sensitive to voltage noise on the trap electrodes than it would be in the  $z$  configuration. Thus, it is desirable to rotate an  $xy$  pair into a  $z$  pair. A procedure for this transformation is shown in Figs. 4d–4f, in which the voltages on the compensation electrodes and endcap electrodes are adjusted in four steps. While it is possible to reduce the transformation to two steps, there is a risk that the ion's displacement along the  $z$  axis exceeds the  $100 \mu\text{m}$  waist of the Doppler-cooling beams. Following the rotation to a  $z$  pair, we observe that if the ion is lost from the trap, another ion can be reloaded directly in this configuration.

We have observed that only a single ion can be loaded in the  $z$  configuration, but in the  $xy$

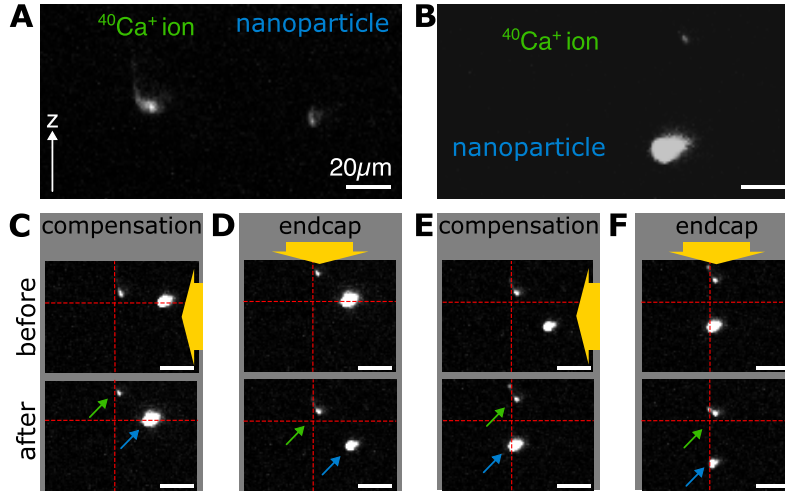


Figure 4: Ion-nanoparticle configurations. The  $z$  axis points in the same direction in all images. (a) EM-CCD images of the  $xy$  and (b)  $z$  configurations. (c) Starting from an  $xy$  pair, we decrease the compensation-electrode voltages that have been used to displace the nanoparticle from the trap center. As a result, the nanoparticle shifts towards the center of the trap, and the ion is repelled along the axis of weakest confinement, which is the  $z$  axis here. (d) The voltage on one endcap is increased to compensate for this shift; both particles shift away from that endcap. (e) The compensation-electrode voltages are decreased further until the nanoparticle lies on the  $z$  axis. (f) The endcap voltage is increased further until the ion is at the origin.

configuration, we can co-trap two ions with a nanoparticle, as shown in Fig. 1d. To achieve this, the energy of the ablation laser pulse is increased by 10%, to 0.55 mJ; the other co-trapping parameters remain unchanged. We have never observed more than two ions co-trapped with the nanoparticle, but we expect that this should be possible with improvements to the experimental setup. In particular, when operated in the co-trapping regime, our trap currently dissipates much more power than a typical linear Paul trap, which could be improved with a smaller ion-electrode spacing. Co-trapping multiple ions with a nanoparticle is an interesting prospect as one can couple the nanoparticle to different collective motional modes of the trapped ions, which may offer advantages due to noise suppression (30) or due to the mode frequency.

## Conclusion and outlook

Calcium ions and a charged silica nanoparticle have been simultaneously confined in a dual-frequency Paul trap. We have studied the ion–nanoparticle pair stability as function of the two RF amplitudes, developed a reliable procedure for loading the trap, and demonstrated a method to swap between different geometric configurations. In-situ charging of the trapped nanoparticle is a necessary step to reduce the slow-field amplitude to a level that permits ion trapping. The mismatch of six orders of magnitude between the particle’s charge-to-mass ratios leads to a differential response to static electric fields, which we found to be beneficial for tuning the ion–nanoparticle separation and maximizing ion-loading efficiencies.

Our results lay the groundwork for a hybrid system in which a motional state of a nanoparticle is coupled to external or internal degrees of freedom of trapped ions, with prospects for generating quantum-mechanical states of levitated macroscopic objects (31). While the center-of-mass motional frequencies of nanoparticles in ion traps lie in the kilohertz regime, ro-vibrational modes have megahertz frequencies (32) similar to those of the ions’ center-of-mass motion, enabling both resonant (33) and dispersive couplings (34). Such a hybrid system has been achieved by coupling single superconducting qubits to a piezoelectric resonator (35), a surface-acoustic-wave resonator (36), and a bulk-acoustic-wave resonator (37); the qubit serves to generate and probe quantum states of motion of the resonator (38). Building on these pioneering results, levitated particles offer the novel prospect of preparing quantum mechanical superpositions with a spatial extent larger than the mechanical oscillator itself.

## Acknowledgments

We thank Giovanni Cerchiari and Elisa Soave for helpful discussions.

**Funding:** This research was supported by the Austrian Science Fund (FWF) under grants I5540, W1259 and Y951.

## References

1. R. E. March, J. F. J. Todd, *Quadrupole Ion Trap Mass Spectrometry* (Wiley-Interscience, Hoboken, New Jersey, 2005), second edn.
2. S. Willitsch, *Int. Rev. Phys. Chem.* **31**, 175 (2012).
3. D. Wineland, *et al.*, *J. Res. Natl. Inst. Stand. Technol.* **103**, 259 (1998).
4. D. Leibfried, R. Blatt, C. Monroe, D. Wineland, *Rev. Mod. Phys.* **75**, 281 (2003).
5. C. D. Bruzewicz, J. Chiaverini, R. McConnell, J. M. Sage, *Appl. Phys. Rev.* **6**, 021314 (2019).
6. P. Nagornykh, J. E. Coppock, J. P. J. Murphy, B. E. Kane, *Phys. Rev. B* **96**, 035402 (2017).
7. D. Budker, *et al.*, *PRX Quantum* **3**, 010330 (2022).
8. R. Wester, *J. Phys. B* **42**, 154001 (2009).
9. D. J. Larson, J. C. Bergquist, J. J. Bollinger, W. M. Itano, D. J. Wineland, *Phys. Rev. Lett.* **57**, 70 (1986).
10. D. Kielpinski, *et al.*, *Phys. Rev. A* **61**, 032310 (2000).
11. P. O. Schmidt, *et al.*, *Science* **309**, 749 (2005).
12. F. Wolf, *et al.*, *Nature* **530**, 457 (2016).
13. C.-w. Chou, *et al.*, *Nature* **545**, 203 (2017).
14. M. Sinhal, Z. Meir, K. Najafian, G. Hegi, S. Willitsch, *Science* **367**, 1213 (2020).
15. H. Dehmelt, *Phys. Scr.* **1995**, 423 (1995).

16. D. Trypogeorgos, C. J. Foot, *Phys. Rev. A* **94**, 023609 (2016).
17. N. Leefer, *et al.*, *Hyperfine Interact.* **238**, 12 (2016).
18. L. Dania, D. S. Bykov, F. Goschin, M. Teller, T. E. Northup, Ultra-high quality factor of a levitated nanomechanical oscillator (2023).
19. D. J. Berkeland, J. D. Miller, J. C. Bergquist, W. M. Itano, D. J. Wineland, *J. Appl. Phys.* **83**, 5025 (1998).
20. C. Foot, D. Trypogeorgos, E. Bentine, A. Gardner, M. Keller, *Int. J. Mass Spectrom.* **430**, 117 (2018).
21. P. Asenbaum, S. Kuhn, S. Nimmrichter, U. Sezer, M. Arndt, *Nat. Commun.* **4**, 2743 (2013).
22. S. Kuhn, *et al.*, *Nano Lett.* **15**, 5604 (2015).
23. D. S. Bykov, P. Mestres, L. Dania, L. Schmöger, T. E. Northup, *Appl. Phys. Lett.* **115**, 034101 (2019).
24. L. Dania, D. S. Bykov, M. Knoll, P. Mestres, T. E. Northup, *Phys. Rev. Research* **3**, 013018 (2021).
25. A. N. Vamivakas, *et al.*, *Opt. Lett.* **32**, 970 (2007).
26. F. Xiong, *et al.*, *Phys. Rev. Appl.* **16**, L011003 (2021).
27. D. S. Bykov, L. Dania, F. Goschin, T. E. Northup, *Optica* **10**, 438 (2023).
28. S. Gulde, *et al.*, *Appl. Phys. B* **73**, 861 (2001).
29. R. Hendricks, D. Grant, P. Herskind, A. Dantan, M. Drewsen, *Appl. Phys. B* **88**, 507 (2007).
30. B. E. King, *et al.*, *Phys. Rev. Lett.* **81**, 1525 (1998).

31. C. Gonzalez-Ballester, M. Aspelmeyer, L. Novotny, R. Quidant, O. Romero-Isart, *Science* **374**, 168 (2021).
32. T. M. Hoang, *et al.*, *Phys. Rev. Lett.* **117**, 123604 (2016).
33. Y. Chu, *et al.*, *Science* **358**, 199 (2017).
34. P. Arrangoiz-Arriola, *et al.*, *Nature* **571**, 537 (2019).
35. A. D. O'Connell, *et al.*, *Nature* **464**, 697 (2010).
36. R. Manenti, *et al.*, *Nat. Commun.* **8**, 975 (2017).
37. M. Bild, *et al.*, *Science* **380**, 274 (2023).
38. Y. Chu, S. Gröblacher, *Appl. Phys. Lett.* **117**, 150503 (2020).